

Enabling four-dimensional conformal hybrid meshing with cubic pyramids

Miroslav S. Petrov · Todor D. Todorov ·
Gage S. Walters · David M. Williams ·
Freddie D. Witherden

Received: date / Accepted: date

Abstract The main purpose of this article is to develop a novel refinement strategy for four-dimensional hybrid meshes based on cubic pyramids. This optimal refinement strategy subdivides a given cubic pyramid into a conforming set of congruent cubic pyramids and invariant bipentatopes. The theoretical properties of the refinement strategy are rigorously analyzed and evaluated. In addition, a new class of fully symmetric quadrature rules with positive weights are generated for the cubic pyramid. These rules are capable of exactly integrating polynomials with degrees up to 12. Their effectiveness is successfully demonstrated on polynomial and transcendental functions. Broadly speaking, the refinement strategy and quadrature rules in this paper open new avenues for four-dimensional hybrid meshing, and space-time finite element methods.

Keywords 4D hybrid meshes · cubic pyramids · bipentatopes · pentatopes · optimal refinement strategy · quadrature

Mathematics Subject Classification (2010) 52B11 · 65N30 · 65N50 · 65D30 · 65D32

M. Petrov
Department of Technical Mechanics, Technical University, 5300 Gabrovo, Bulgaria

T. Todorov
Department of Mathematics, Informatics and Natural Sciences, Technical University, 5300 Gabrovo, Bulgaria

G. Walters
Department of Mechanical Engineering, The Pennsylvania State University, University Park, Pennsylvania 16802, USA

D. Williams
Department of Mechanical Engineering, The Pennsylvania State University, University Park, Pennsylvania 16802, USA
E-mail: david.m.williams@psu.edu

F. Witherden
Department of Ocean Engineering, Texas A&M University, College Station, Texas 77843, USA

1 Introduction

The classical way of solving nonstationary boundary value problems applies separate discretizations in space and time. One promising alternative to this approach is the finite element method with full space-time discretization. In principle, this method can be very effective for solving hyperbolic and parabolic problems. Some basic examples of space-time methods can be found in [35, 36, 38] and the recent survey of Langer and Steinbach [21]. In addition, a representative example of this work is provided by Dumont et al. [17] who developed a space-time finite element method to solve elastodynamics problems. Since the dynamics problem in [17] involves a three-dimensional spatial body, the authors have constructed four-dimensional meshes. Dumont et al. have not developed general, unstructured triangulations in four-dimensional domains. Rather, they firstly make a spatial triangulation and then extend the domain in the temporal direction to obtain a four-dimensional finite element triangulation. A similar approach for generating four-dimensional simplex meshes has been employed by Neumüller and Karabelas in [25]. A detailed survey of four-dimensional structured and unstructured simplicial meshing techniques is provided by Caplan [8] and Frontin et al. [18]. Finally, examples of refinement strategies for high-dimensional simplicial meshes have been developed in the work of Brandts et al. [6], and Korotov and Křížek [20].

There have been virtually no efforts to develop four-dimensional hybrid meshes. However, in the last few decades, there has been interest in the development of hybrid *three-dimensional* meshes [5, 7], with some important work being contributed by Yamakawa and coworkers [41, 42, 43, 44, 45]. In [45], Yamakawa and Shimada developed a procedure for creating hexahedron dominant meshes in order to model thin-wall structures. Additionally, Yamakawa et al. described a conforming coupling between hexahedron and tetrahedron meshes by using square pyramid interface elements [43], and using triangular prism interface elements [41]. The conforming coupling of hexahedra and tetrahedra via pyramids has been discussed independently by Meshkat and Talmor [24], and Devloo et al. [16]. In addition, Pantano and Averill [28] have used a non-conforming, penalty-based procedure to couple independently modeled three-dimensional finite element meshes. Similar non-conforming techniques using mortar elements have been explored by Maday et al. [22] and Seshaiyer and Suri [32]. Furthermore, hybrid non-conforming hexahedral-tetrahedral meshes have been examined by Reberol and Lévy [31]. Unfortunately, these non-conforming meshes are incompatible with most standard finite element methods, with the exception of discontinuous Galerkin methods. Evidently, the most convenient way to unify independently created finite element meshes is through the conforming coupling of the elements in the interface subdomain. This strongly motivates the importance of transitional elements, such as pyramidal and prismatic elements.

Let us briefly review previous efforts to analyze transitional elements. Evidently, the three-dimensional prismatic elements are relatively straightforward to analyze, as they can be constructed by forming tensor products between line

segments and triangles, whereas, a similar procedure is impossible for pyramids. As a result, prismatic elements inherit their interpolation and quadrature procedures from well-established 1D/2D procedures, and researchers have primarily focused their attention on pyramids. The pioneering work on pyramids was performed by Bedrosian [4] in the early nineties. He was the first researcher who explained the role of pyramidal elements for coupling different kinds of meshes, and developed the first interpolation and integration procedures. A number of researchers have followed in Bedrosian's footsteps [1, 5, 9, 10, 11, 12, 13, 19]. In particular, Bergot et al. [5] performed a deep analysis of the interpolation properties of pyramidal elements. Chan and Warburton extended this work, developing alternative sets of basis functions [11, 12], analyzing the numerical stability of interpolation points [9], and deriving trace inequalities [10]. Furthermore, Gillette [19] recently used techniques from finite element exterior calculus [2, 3] to construct serendipity-type basis functions on pyramids. Quadrature formulas on pyramidal elements have been created and analyzed in [5, 26, 40]. The error estimates arising from the quadrature rules of Bergot et al. [5] have been improved by Nigam and Phillips [26] in order to obtain the classical rate of convergence for second-order boundary value problems. However, the best set of rules to date (in terms of integration strength for a minimum number of points) was identified by Witherden and Vincent in [40].

Now, let us return our attention to four-dimensional space. It turns out that the three-dimensional definitions of transitional elements do not extend to higher dimensions. For example, while the triangular prism provides a conforming interface between the hexahedron and the tetrahedron in three dimensions, its analog in four dimensions (the tetrahedral prism) does *not* provide a conforming interface between the tesseract and the pentatope. This immediately follows from the fact that the tetrahedral prism has two tetrahedral facets and four triangular prismatic facets, and therefore it cannot conformally interface with the tesseract. In a similar fashion, the cubic pyramid (the four-dimensional analog of the square pyramid) has one hexahedral facet and six square pyramidal facets, and therefore it cannot conformally interface with the pentatope. Fortunately, the lack of transitional elements between tesseracts and pentatopes does not completely prevent the formulation of hybrid meshes in four dimensions. We will show that it is still possible to build hybrid meshes using tesseract, cubic pyramid, and pentatopal elements. We note that some basic geometric properties of these elements are discussed in the work of Coxeter [14, 15], Sommerville [23], and Zamboj [46].

The main goals of this paper are: i) to develop conforming hybrid four-dimensional meshes, ii) to create an optimal refinement strategy for these meshes, and iii) to develop numerical integration procedures on the elements of these meshes. The major contributions of the paper are summarized as follows. First, we identify a four-dimensional conforming coupling between tesseract elements and cubic pyramid elements. Next, the tesseract and cubic pyramid elements are subdivided, while maintaining conformity. Evidently, while the tesseracts can be uniformly subdivided into smaller tesseracts, the

cubic pyramids cannot be subdivided into smaller cubic pyramids without leaving gaps. Therefore, in the refinement strategy for the cubic pyramids, we use a combination of congruent cubic pyramids *and* invariant bipentatopes. A simple two-level refinement tree is obtained. The theoretical properties of the refinement strategy are thoroughly analyzed. The proposed theoretical results cannot be improved, otherwise the cubic pyramid would be invariant with a one-level refinement tree, which is obviously not the case. Finally, we conclude our work by developing numerical integration procedures for the cubic pyramid elements. We note that, while such procedures are already well-established for the tesseract and pentatope elements [18,39], they have yet to be developed for cubic pyramid elements.

The format of this paper is as follows. In Section 2, we introduce some standard notation and terminology. In Section 3, we formulate new hybrid meshes of tesseract, cubic pyramid, and bipentatope elements, along with a non-degenerate mesh refinement strategy. In Section 4, we develop theoretical results which govern the hybrid meshes. In Section 5, we introduce a new set of fully symmetric quadrature rules for cubic pyramid elements. Finally, in Section 6, we summarize the main conclusions of the paper.

2 Preliminary concepts

2.1 Background and motivation

The four-dimensional space \mathbb{R}^4 has unique geometric properties which cannot be found in other multidimensional Euclidean spaces excluding the two-dimensional one. This fact can be illustrated by comparing the three- and four-dimensional spaces. It is well-known that the 3-cube cannot be triangulated by standard tetrahedra (i.e. cube corners) [20]. Rather, the cube is usually triangulated into five simplices, four of which are standard tetrahedra and one of which is a regular tetrahedron. Additionally, it is impossible to triangulate the standard tetrahedron with standard tetrahedra. Instead, there exists a partition of the standard tetrahedron into six standard tetrahedra and one regular tetrahedron [37]. Interestingly enough, these principles do not extend to the four-dimensional case. Petrov and Todorov [29] have proved that each tesseract can be divided into standard pentatopes (i.e. tesseract corners), and each standard pentatope can be partitioned into standard pentatopes. The latter fact means that an arbitrary 4D *canonical* domain can be divided into standard pentatopes [29], which are the most convenient elements from a computational point of view. The authors have tested six- and eight-dimensional hypercubes for such properties, but without success. Therefore, given its useful properties, more attempts to explore and analyze four-dimensional space are certainly warranted.

In what follows, we will introduce some useful definitions which facilitate our subsequent discussions of \mathbb{R}^4 .

2.2 Definitions

Definition 1 A simply connected domain in \mathbb{R}^4 is called canonical if there exists a conforming partition of the domain into tesseracts (4-cubes).

Definition 2 Each n -dimensional hypercube can be divided into $2n$ $(n - 1)$ -hypercube pyramids. These pyramids are called canonical pyramids.

Definition 3 Let Ω be a nondegenerated polytope in \mathbb{R}^4 , and T_i , $i = 1, 2, \dots, k$, be 4-dimensional finite elements. The triangulation

$$\tau = \left\{ T_i \subset \mathbb{R}^4 \mid \Omega = \bigcup_{i=1}^k T_i \right\},$$

of the polytope Ω is said to be consistent if T_i and T_j , $1 \leq i < j \leq k$, share nothing other than the empty set, a vertex, an edge or an ℓ -dimensional facet, $\ell = 2, 3$.

Definition 4 The polytope

$$T_{-i} = [t_1, t_2, \dots, t_{i-1}, t_{i+1}, \dots, t_{n+1}], \quad i = 2, \dots, n,$$

related to the vertex t_i is obtained from the polytope $T = [t_1, t_2, \dots, t_{n+1}]$, $n \in \mathbb{N}$ by removing the vertex t_i . The polytopes T_{-1} and $T_{-(n+1)}$ are defined in a similar fashion as

$$T_{-1} = [t_2, t_3, \dots, t_{n+1}], \quad T_{-(n+1)} = [t_1, t_2, \dots, t_n].$$

Definition 5 The polytopes T_1 and T_2 are congruent if one of them can be obtained from the other by applying a linear transformation

$$T_2 = \underline{b} + cQT_1,$$

where $c \neq 0$ is a scaling factor, \underline{b} is a translation vector, and Q is an orthogonal matrix.

Definition 6 We say that two polytopes T_1 and T_2 are from the same class if they are congruent.

The class

$$[K] = \{T \subset \mathbb{R}^4 \mid T \cong K\},$$

consists of all equivalent pyramids to the pyramid K in \mathbb{R}^4 with respect to the congruence relation.

Definition 7 A polytope T is said to be invariant concerning a refinement strategy \mathcal{A} if all elements of $\mathcal{A}T$ belong to $[T]$.

Definition 8 The degeneracy measure of an arbitrary pyramid $K = [k_1, k_2, \dots, k_{n+1}]$ is equal to

$$\delta(K) = \frac{h(K) \cdot \text{vol}(\partial K)}{8 \cdot \text{vol}(K)},$$

where $h(K)$ is the diameter of K .

Here, we use $\text{vol}(T)$ and $\text{vol}(\partial T)$ instead of $\text{vol}_4(T)$ and $\text{vol}_3(\partial T)$ in order to avoid complicated notation.

2.3 Reference elements

In this section, we introduce a set of convenient reference elements in \mathbb{R}^4 . We review the important properties of these elements, including their vertex locations, integration limits, and orthonormal polynomial bases.

In order to prepare our discussion of the reference elements, let us briefly review the definition of an orthonormal basis. Broadly speaking, the basis maintains the following key property

$$\int_{\Omega} \psi_{ijkq}(\mathbf{x}) \psi_{rstv}(\mathbf{x}) d\mathbf{x} = \delta_{ir} \delta_{js} \delta_{kt} \delta_{qv},$$

where δ_{ir} is the Kronecker delta. The orthonormal basis functions of degree p have the form

$$\psi_{ijkq}(\mathbf{x}) = \zeta_{ijkq} \hat{P}_i^{(\alpha_1, \beta_1)}(a) \hat{P}_j^{(\alpha_2, \beta_2)}(b) \hat{P}_k^{(\alpha_3, \beta_3)}(c) \hat{P}_q^{(\alpha_4, \beta_4)}(d) f(\mathbf{x}),$$

where $i + j + k + q \leq p$, $a = a(x_1, x_4)$, $b = b(x_2, x_4)$, $c = c(x_3, x_4)$, $d = d(x_4)$, and $f = f(\mathbf{x})$ are functions depending on the element type, ζ_{ijkq} , $\alpha_1, \dots, \alpha_4$ and β_1, \dots, β_4 are constants, and $\hat{P}_n^{(\alpha, \beta)}$ are the 1D orthonormal Jacobi polynomials defined as

$$\hat{P}_n^{(\alpha, \beta)}(x_1) = \frac{P_n^{(\alpha, \beta)}(x_1)}{\sqrt{\frac{2^{\alpha+\beta+1} (n+\alpha)!(n+\beta)!}{2n+\alpha+\beta+1 n!(n+\alpha+\beta)!}}}.$$

Here, the functions $P_n^{(\alpha, \beta)}$ are the well-known orthogonal Jacobi polynomials, which themselves are *not* orthonormal. The scale factor under the square root operator provides the desired normalization.

It is convenient to omit the Jacobi polynomial superscripts when $\alpha = \beta = 0$. Consequently, we frequently write \hat{P}_n in place of $\hat{P}_n^{(0,0)}$.

Now, let us turn our attention to the definitions of the reference elements.

2.3.1 Tesseract

Consider the reference tesseract T^* centered at the origin, having edge length $l[T^*] = 2$. The vertices are defined such that

$$T^* = \left[t_1(-1, -1, -1, -1), t_2(-1, 1, -1, -1), t_3(-1, -1, -1, 1), t_4(1, -1, -1, -1), \right. \\ t_5(-1, 1, -1, 1), t_6(1, -1, -1, 1), t_7(1, 1, -1, -1), t_8(1, 1, -1, 1), \\ t_9(-1, -1, 1, 1), t_{10}(-1, 1, 1, 1), t_{11}(-1, -1, 1, -1), t_{12}(1, -1, 1, 1), \\ \left. t_{13}(-1, 1, 1, -1), t_{14}(1, -1, 1, -1), t_{15}(1, 1, 1, 1), t_{16}(1, 1, 1, -1) \right],$$

as shown in Figure 1. The volume is $\text{vol}(T^*) = 16$ and it is straightforward to define bounds of integration

$$\int_{-1}^1 \int_{-1}^1 \int_{-1}^1 \int_{-1}^1 dx_1 dx_2 dx_3 dx_4 = 16.$$

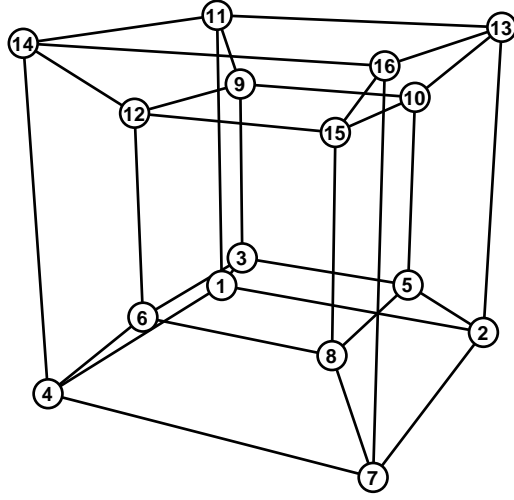


Fig. 1: The reference tesseract T^* .

Trivially, the orthonormal basis inside of the reference tesseract is given by

$$\psi_{ijkq}(\mathbf{x}) = \hat{P}_i(a) \hat{P}_j(b) \hat{P}_k(c) \hat{P}_q(d),$$

where $a = x_1$, $b = x_2$, $c = x_3$, and $d = x_4$.

2.3.2 Cubic pyramid

Consider the reference cubic pyramid K^* centered at the origin, having edge length $l[K^*] = 2$. The vertices are defined such that

$$K^* = \left[k_1(-1, -1, -1, -1), k_2(-1, 1, -1, -1), k_3(-1, -1, 1, -1), k_4(1, -1, -1, -1), \right. \\ \left. k_5(-1, 1, 1, -1), k_6(1, -1, 1, -1), k_7(1, 1, -1, -1), k_8(1, 1, 1, -1), \right. \\ \left. k_9(0, 0, 0, 0) \right],$$

as shown in Figure 2. The volume of the cubic pyramid is 1/8th of the tesseract, or equivalently $\text{vol}(K^*) = \frac{Ah}{4}$ where $A = 8$ is the area of the hexahedron base and $h = 1$ is the height of the cubic pyramid. Based on the vertices of K^* , the integration bounds for the cubic pyramid are

$$\int_{-1}^0 \int_{x_4}^{-x_4} \int_{x_4}^{-x_4} \int_{x_4}^{-x_4} dx_1 dx_2 dx_3 dx_4 = 2.$$

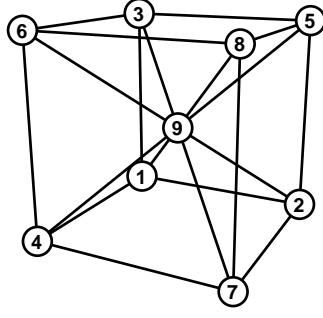


Fig. 2: The reference cubic pyramid K^* .

The orthonormal polynomial basis for the cubic pyramid is found to be

$$\psi_{ijkq}(\mathbf{x}) = \sqrt{2^{\mu_{ijk}+1}} \hat{P}_i(a) \hat{P}_j(b) \hat{P}_k(c) \hat{P}_q^{(\mu_{ijk},0)}(d) (-x_4)^{i+j+k}, \quad (1)$$

where $a = -\frac{x_1}{x_4}$, $b = -\frac{x_2}{x_4}$, $c = -\frac{x_3}{x_4}$, $d = 2x_4 + 1$, and $\mu_{ijk} = 2i + 2j + 2k + 3$.

2.3.3 Bipentatope

Consider the reference bipentatope P^* having edge length $l[P^*] = 1$. This element is also frequently called the tetrahedral bipyramid. The vertices are defined such that

$$P^* = \left[p_1 \left(\frac{1}{2}, \frac{1}{2}, \frac{1}{2}, -\frac{1}{2} \right), p_2 \left(\frac{1}{2}, \frac{1}{2}, -\frac{1}{2}, -\frac{1}{2} \right), p_3 \left(-\frac{1}{2}, \frac{1}{2}, -\frac{1}{2}, -\frac{1}{2} \right), p_4 \left(-\frac{1}{2}, \frac{1}{2}, \frac{1}{2}, -\frac{1}{2} \right), \right. \\ \left. p_5 (0, 1, 0, -1), p_6 (0, 0, 0, -1) \right],$$

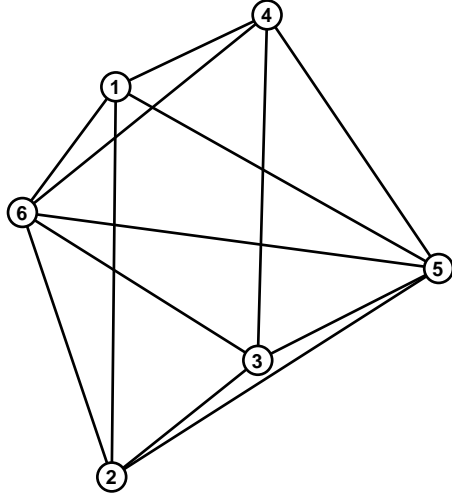
as shown in Figure 3. The reference bipentatope volume is $\text{vol}(P^*) = \frac{1}{24}$.

In order to facilitate interpolation and integration, the reference bipentatope can be divided into two pentatopes, as shown in Figure 4. There exists a convenient mapping from these pentatopes onto the standard pentatope S^* shown in Figure 5. We note that S^* has the following vertices

$$S^* = \left[s_1 (1, -1, -1, -1), s_2 (-1, 1, -1, -1), s_3 (-1, -1, 1, -1), s_4 (-1, -1, -1, 1), \right. \\ \left. s_5 (-1, -1, -1, -1) \right].$$

The standard pentatope volume is $\text{vol}(S^*) = \frac{2}{3}$ and the bounds of integration are

$$\int_{-1}^1 \int_{-1}^{-1-x_4} \int_{-1}^{-1-x_3-x_4} \int_{-1}^{-1-x_2-x_3-x_4} dx_1 dx_2 dx_3 dx_4 = \frac{2}{3}.$$

Fig. 3: The reference bipentatope P^* .

The orthonormal polynomial basis takes the following form

$$\begin{aligned} \psi_{ijkq}(\mathbf{x}) = & 4\hat{P}_i(a) \hat{P}_j^{(2i+1,0)}(b) \hat{P}_k^{(2i+2j+2,0)}(c) \hat{P}_q^{(2i+2j+2k+3,0)}(d) \\ & \times (1-b)^i (1-c)^{i+j} (1-d)^{i+j+k}, \end{aligned} \quad (2)$$

where $a = -2\frac{x_1+1}{x_2+x_3+x_4+1} - 1$, $b = -2\frac{1+x_2}{x_3+x_4} - 1$, $c = 2\frac{1+x_3}{1-x_4} - 1$, and $d = x_4$.

Lastly, we consider the following rescaled and shifted version of the standard pentatope

$$\mathcal{S}^* = [s_1^*(1, 0, 0, 0), s_2^*(0, 1, 0, 0), s_3^*(0, 0, 1, 0), s_4^*(0, 0, 0, 1), s_5^*(0, 0, 0, 0)],$$

where by inspection

$$\mathcal{S}^* = \frac{1}{2}\mathcal{S}^* + (1, 1, 1, 1).$$

This reference element has been used by many authors [6, 29] due to its mathematical simplicity and convenience. It is frequently referred to as the ‘cube corner’. Its volume is $\text{vol}(\mathcal{S}^*) = \frac{1}{24}$ and the bounds of integration are

$$\int_0^1 \int_0^{1-x_4} \int_0^{1-x_3-x_4} \int_0^{1-x_2-x_3-x_4} dx_1 dx_2 dx_3 dx_4 = \frac{1}{24}.$$

The orthonormal polynomial basis on the cube corner can be obtained by a simple linear transformation of the basis in Eq. (2).

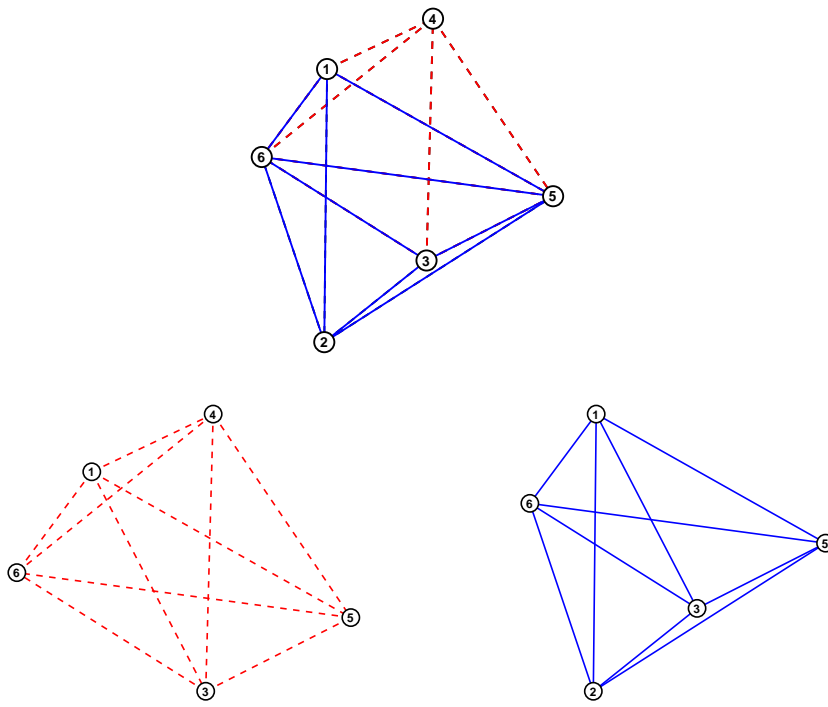


Fig. 4: A subdivision of the reference bipentatope into two pentatopes.

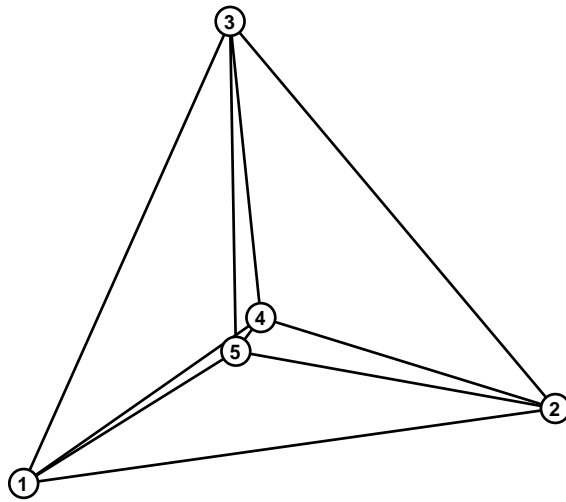


Fig. 5: The standard pentatope S^* .

3 Hybrid meshes of tesseracts, cubic pyramids, and bipentatopes

In this section, we introduce a set of hybrid meshes by constructing the following domain model. Let Ω be a four-dimensional canonical domain. The domain Ω is partitioned into two subdomains Ω_1 and Ω_2 , which are also canonical. We suppose that $\tilde{\tau}_0$ and $\hat{\tau}_0$ are tesseract triangulations of Ω_1 and Ω_2 such that all elements of both triangulations form a conforming tesseract triangulation τ_0 of the domain Ω . We define the boundary layers in the subdomains Ω_1 and Ω_2 by

$$B_1 = \{T \in \Omega_1 \mid \dim(\partial T \cap \Omega_{12}) = 3\},$$

$$B_2 = \{T \in \Omega_2 \mid \dim(\partial T \cap \Omega_{12}) = 3\}, \quad \Omega_{12} = \Omega_1 \cap \Omega_2.$$

Furthermore, we construct a hybrid mesh so that Ω_1 is partitioned by tesseract elements and Ω_2 is partitioned by cubic pyramid elements. Our main goal is to establish a conforming coupling between the different kinds of elements in the boundary layers of both subdomains. Additionally, we need a refinement strategy for both groups of elements with as small as possible number of classes and as small as possible measure of degeneracy for the pyramidal elements. We restrict ourselves to refinement strategies dividing the edges of each element into two parts. We anticipate that such strategies will be very useful in multigrid and/or adaptive-quadrature procedures.

We will now define a refinement algorithm for creating nested hierarchical hybrid triangulations in five steps:

- (r_1) The tesseract triangulations of Ω , denoted by $\tilde{\tau}_0$, $\hat{\tau}_0$ and $\tau_0 = \tilde{\tau}_0 \cup \hat{\tau}_0$ are constructed. We denote this partition operator by \mathcal{R} .
- (r_2) Each element T of $\tilde{\tau}_0$ is uniformly divided into sixteen smaller tesseracts. We denote this partition operator by \mathcal{E} . Evidently, this operator's definition is straightforward, and does not need to be explicitly stated.
- (r_3) Each element T of $\hat{\tau}_0$ is divided into eight cubic pyramids by connecting the cubic facets of each element to its centroid. We denote this partition operator by \mathcal{B} . It is given explicitly by

$$\begin{aligned} \mathcal{B}T^* = \{ & K_1[t_1, t_2, t_3, t_4, t_5, t_6, t_7, t_8, t_0], K_2[t_1, t_3, t_4, t_6, t_9, t_{11}, t_{12}, t_{14}, t_0], \\ & K_3[t_9, t_{10}, t_{11}, t_{12}, t_{13}, t_{14}, t_{15}, t_{16}, t_0], K_4[t_2, t_5, t_7, t_8, t_{10}, t_{13}, t_{15}, t_{16}, t_0], \\ & K_5[t_4, t_6, t_7, t_8, t_{12}, t_{14}, t_{15}, t_{16}, t_0], K_6[t_1, t_2, t_3, t_5, t_9, t_{10}, t_{11}, t_{13}, t_0], \\ & K_7[t_1, t_2, t_4, t_7, t_{11}, t_{13}, t_{14}, t_{16}, t_0], K_8[t_3, t_5, t_6, t_8, t_9, t_{10}, t_{12}, t_{15}, t_0] \}. \end{aligned}$$

One of the resulting cubic pyramids K_7 is shown in Figure 6. Note: K_7 is equivalent to K^* , which is a canonical pyramid.

- (r_4) The elements of $\mathcal{B}\hat{\tau}_0$ are further subdivided by the partition operator \mathcal{L} , which is defined below.
- (r_5) Steps 2–4 are performed repeatedly until the desired level of mesh refinement is obtained. These refinement steps are denoted by the operator \mathcal{H} .

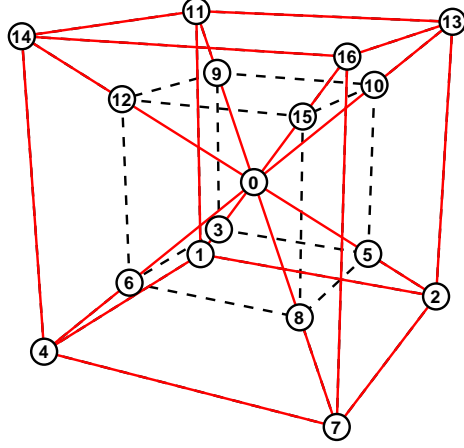


Fig. 6: The cubic pyramid K_7 belonging to the decomposition \mathcal{BT}^* .

Now, let us turn our attention to formulating an explicit definition for the partition operator \mathcal{L}

$$\mathcal{L}X = \begin{cases} \mathcal{D}X, & \text{if } X \text{ is a cubic pyramid} \\ \mathcal{M}X, & \text{if } X \text{ is a bipentatope.} \end{cases}$$

It remains for us to define the operators \mathcal{D} and \mathcal{M} . The operator \mathcal{D} can be defined as follows

$$\mathcal{D}K^* = \left\{ \left\{ \mathbb{K}_1[k_1, k_{10}, k_{11}, k_{12}, k_{13}, k_{14}, k_{15}, k_{16}, k_{21}], \mathbb{K}_2[k_2, k_{10}, k_{13}, k_{14}, k_{15}, k_{17}, k_{18}, k_{19}, k_{20}], \right. \right. \\ \mathbb{K}_3[k_4, k_{12}, k_{14}, k_{15}, k_{21}, k_{26}, k_{27}, k_{28}, k_{29}], \mathbb{K}_4[k_7, k_{14}, k_{15}, k_{18}, k_{19}, k_{27}, k_{28}, k_{34}, k_{35}], \\ \mathbb{K}_5[k_3, k_{11}, k_{13}, k_{15}, k_{21}, k_{22}, k_{23}, k_{24}, k_{25}], \mathbb{K}_6[k_5, k_{13}, k_{15}, k_{17}, k_{19}, k_{22}, k_{24}, k_{30}, k_{31}], \\ \mathbb{K}_7[k_6, k_{15}, k_{21}, k_{23}, k_{24}, k_{26}, k_{28}, k_{32}, k_{33}], \mathbb{K}_8[k_8, k_{15}, k_{19}, k_{24}, k_{28}, k_{30}, k_{32}, k_{34}, k_{36}], \\ \left. \mathbb{K}_9[k_9, k_{16}, k_{20}, k_{25}, k_{29}, k_{31}, k_{33}, k_{35}, k_{36}], \mathbb{K}_{10}[k_{15}, k_{16}, k_{20}, k_{25}, k_{29}, k_{31}, k_{33}, k_{35}, k_{36}] \right\}, \\ \left\{ P_1[k_{15}, k_{21}, k_{23}, k_{24}, k_{25}, k_{33}], P_2[k_{11}, k_{13}, k_{15}, k_{16}, k_{21}, k_{25}], P_3[k_{12}, k_{14}, k_{15}, k_{16}, k_{21}, k_{29}], \right. \\ P_4[k_{15}, k_{21}, k_{26}, k_{28}, k_{29}, k_{33}], P_5[k_{15}, k_{24}, k_{28}, k_{32}, k_{33}, k_{36}], P_6[k_{14}, k_{15}, k_{27}, k_{28}, k_{29}, k_{35}], \\ P_7[k_{15}, k_{19}, k_{28}, k_{34}, k_{35}, k_{36}], P_8[k_{13}, k_{15}, k_{17}, k_{19}, k_{20}, k_{31}], P_9[k_{15}, k_{19}, k_{24}, k_{30}, k_{31}, k_{36}], \\ P_{10}[k_{14}, k_{15}, k_{18}, k_{19}, k_{20}, k_{35}], P_{11}[k_{13}, k_{15}, k_{22}, k_{24}, k_{25}, k_{31}], P_{12}[k_{10}, k_{13}, k_{14}, k_{15}, k_{16}, k_{20}], \\ P_{13}[k_{15}, k_{19}, k_{20}, k_{31}, k_{35}, k_{36}], P_{14}[k_{15}, k_{28}, k_{29}, k_{33}, k_{35}, k_{36}], P_{15}[k_{15}, k_{16}, k_{21}, k_{25}, k_{29}, k_{33}], \\ \left. P_{16}[k_{13}, k_{15}, k_{16}, k_{20}, k_{25}, k_{31}], P_{17}[k_{15}, k_{24}, k_{25}, k_{31}, k_{33}, k_{36}], P_{18}[k_{14}, k_{15}, k_{16}, k_{20}, k_{29}, k_{35}] \right\}.$$

All elements \mathbb{K}_i , $i = 1, 2, \dots, 10$, are cubic pyramids and all elements P_j , $j = 1, 2, \dots, 18$, are bipentatopes. The first nine vertices (above) k_1, k_2, \dots, k_9 are previously defined in the definition of K^* . In addition, the remaining vertices k_{10}, \dots, k_{36} can be defined as follows

$$\begin{aligned}
k_{10} &= \frac{1}{2}(k_1 + k_2), & k_{11} &= \frac{1}{2}(k_1 + k_3), & k_{12} &= \frac{1}{2}(k_1 + k_4), & k_{13} &= \frac{1}{2}(k_1 + k_5), \\
k_{14} &= \frac{1}{2}(k_1 + k_7), & k_{15} &= \frac{1}{2}(k_1 + k_8), & k_{16} &= \frac{1}{2}(k_1 + k_9), & k_{17} &= \frac{1}{2}(k_2 + k_5), \\
k_{18} &= \frac{1}{2}(k_2 + k_7), & k_{19} &= \frac{1}{2}(k_2 + k_8), & k_{20} &= \frac{1}{2}(k_2 + k_9), & k_{21} &= \frac{1}{2}(k_3 + k_4), \\
k_{22} &= \frac{1}{2}(k_3 + k_5), & k_{23} &= \frac{1}{2}(k_3 + k_6), & k_{24} &= \frac{1}{2}(k_3 + k_8), & k_{25} &= \frac{1}{2}(k_3 + k_9), \\
k_{26} &= \frac{1}{2}(k_4 + k_6), & k_{27} &= \frac{1}{2}(k_4 + k_7), & k_{28} &= \frac{1}{2}(k_4 + k_8), & k_{29} &= \frac{1}{2}(k_4 + k_9), \\
k_{30} &= \frac{1}{2}(k_5 + k_8), & k_{31} &= \frac{1}{2}(k_5 + k_9), & k_{32} &= \frac{1}{2}(k_6 + k_8), & k_{33} &= \frac{1}{2}(k_6 + k_9), \\
k_{34} &= \frac{1}{2}(k_7 + k_8), & k_{35} &= \frac{1}{2}(k_7 + k_9), & k_{36} &= \frac{1}{2}(k_8 + k_9).
\end{aligned}$$

The full set of vertices is illustrated in Figure 7. In addition, a few of the individual elements of \mathcal{DK}^* are shown in Figure 8. Finally, several couplings between the cubic pyramid and bipentatope elements are shown in Figure 9.

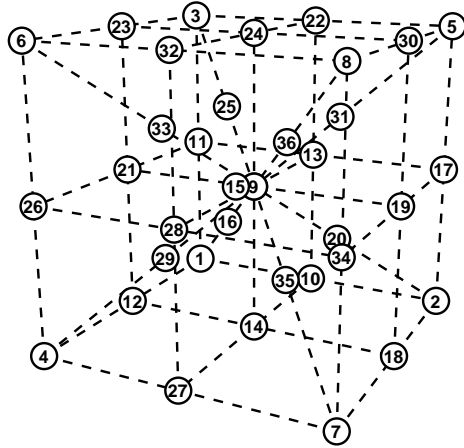


Fig. 7: The cubic pyramid K^* and the full set of vertices for the subdivision operator \mathcal{DK}^* .

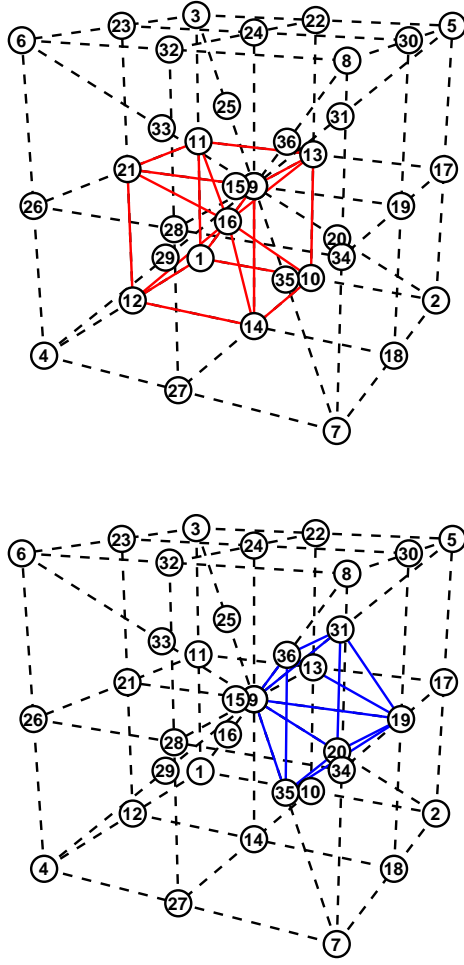


Fig. 8: The cubic pyramid element \mathbb{K}_1 and the bipentatope element P_{13} of the decomposition \mathcal{DK}^* .

Next, the operator \mathcal{M} can be defined as follows

$$\mathcal{MP}^* = \left\{ \begin{aligned} &\mathbb{P}_1[p_5, p_{10}, p_{13}, p_{16}, p_{18}, p_{20}], \mathbb{P}_2[p_6, p_{11}, p_{14}, p_{17}, p_{19}, p_{20}], \mathbb{P}_3[p_8, p_{10}, p_{13}, p_{16}, p_{18}, p_{20}], \\ &\mathbb{P}_4[p_8, p_{11}, p_{14}, p_{17}, p_{19}, p_{20}], \mathbb{P}_5[p_8, p_{16}, p_{17}, p_{18}, p_{19}, p_{20}], \mathbb{P}_6[p_8, p_{13}, p_{14}, p_{16}, p_{17}, p_{20}], \\ &\mathbb{P}_7[p_8, p_{10}, p_{11}, p_{18}, p_{19}, p_{20}], \mathbb{P}_8[p_8, p_{10}, p_{11}, p_{13}, p_{14}, p_{20}], \mathbb{P}_9[p_3, p_8, p_{12}, p_{15}, p_{16}, p_{17}], \\ &\mathbb{P}_{10}[p_4, p_8, p_9, p_{15}, p_{18}, p_{19}], \mathbb{P}_{11}[p_1, p_7, p_8, p_9, p_{10}, p_{11}], \mathbb{P}_{12}[p_2, p_7, p_8, p_{12}, p_{13}, p_{14}], \\ &\mathbb{P}_{13}[p_8, p_{15}, p_{16}, p_{17}, p_{18}, p_{19}], \mathbb{P}_{14}[p_8, p_{12}, p_{13}, p_{14}, p_{16}, p_{17}], \mathbb{P}_{15}[p_7, p_8, p_{10}, p_{11}, p_{13}, p_{14}], \\ &\mathbb{P}_{16}[p_8, p_9, p_{10}, p_{11}, p_{18}, p_{19}] \end{aligned} \right\}.$$

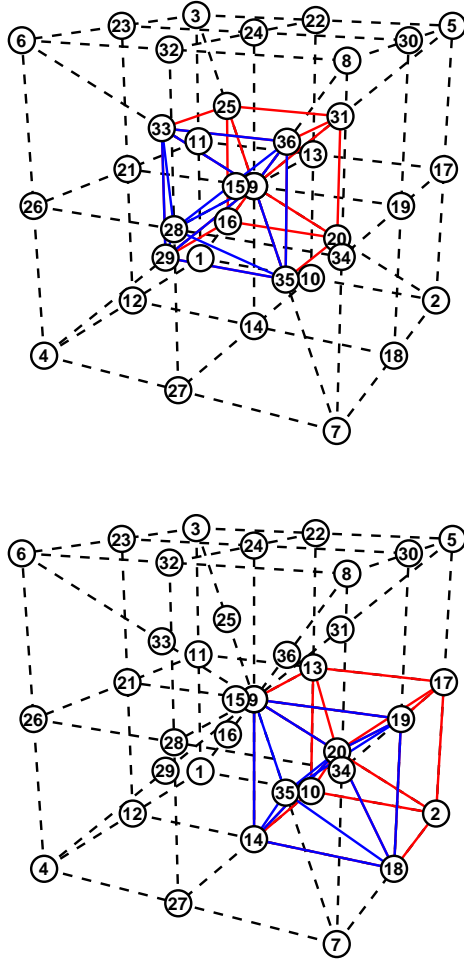


Fig. 9: Couplings between cubic pyramid and bipyramidal elements: \mathbb{K}_{10} and P_{14} (top) and \mathbb{K}_2 and P_{10} (bottom).

All the elements \mathbb{P}_j , $j = 1, 2, \dots, 16$, are bipyramidal. The first six vertices (above) p_1, p_2, \dots, p_6 are previously defined in the definition of P^* . In addition, the remaining vertices p_7, \dots, p_{20} can be defined as follows

$$\begin{aligned}
 p_7 &= \frac{1}{2}(p_1 + p_2), & p_8 &= \frac{1}{2}(p_1 + p_3), & p_9 &= \frac{1}{2}(p_1 + p_4), & p_{10} &= \frac{1}{2}(p_1 + p_5), \\
 p_{11} &= \frac{1}{2}(p_1 + p_6), & p_{12} &= \frac{1}{2}(p_2 + p_3), & p_{13} &= \frac{1}{2}(p_2 + p_5), & p_{14} &= \frac{1}{2}(p_2 + p_6), \\
 p_{15} &= \frac{1}{2}(p_3 + p_4), & p_{16} &= \frac{1}{2}(p_3 + p_5), & p_{17} &= \frac{1}{2}(p_3 + p_6), & p_{18} &= \frac{1}{2}(p_4 + p_5), \\
 p_{19} &= \frac{1}{2}(p_4 + p_6), & p_{20} &= \frac{1}{2}(p_5 + p_6).
 \end{aligned}$$

The full set of vertices is illustrated in Figure 10. In addition, a few of the individual elements of \mathcal{MP}^* are shown in Figure 11.

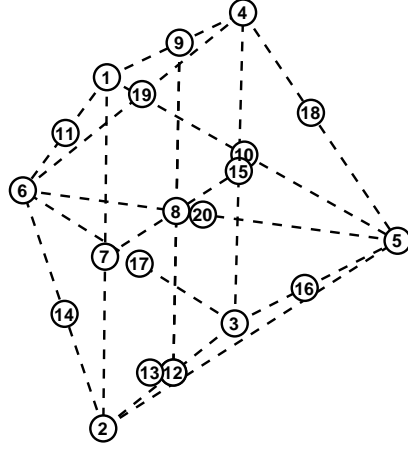


Fig. 10: The bipentatope P^* and the full set of vertices for the subdivision operator \mathcal{MP}^* .

We conclude this section by summarizing the refinement procedure for obtaining hierarchical triangulations below:

$$\begin{aligned}
 \tau_0 &= \mathcal{R}\Omega, & \tau_0 &= \check{\tau}_0 \cup \hat{\tau}_0; \\
 \hat{\tau}_0^* &= \mathcal{B}\hat{\tau}_0, & \tau_0^* &= \check{\tau}_0 \cup \hat{\tau}_0^*; \\
 \check{\tau}_1 &= \mathcal{E}\check{\tau}_0, & \hat{\tau}_1 &= \mathcal{L}\hat{\tau}_0^*, & \tau_1 &= \check{\tau}_1 \cup \hat{\tau}_1; \\
 \check{\tau}_2 &= \mathcal{E}\check{\tau}_1, & \hat{\tau}_2 &= \mathcal{L}\hat{\tau}_1, & \tau_2 &= \check{\tau}_2 \cup \hat{\tau}_2; \\
 \check{\tau}_{k+1} &= \mathcal{E}^k \check{\tau}_1, & \hat{\tau}_{k+1} &= \mathcal{L}^k \hat{\tau}_1, & \tau_{k+1} &= \check{\tau}_{k+1} \cup \hat{\tau}_{k+1}.
 \end{aligned} \tag{3}$$

In accordance with (3), we can explicitly define the partition operator $\mathcal{H} : \tau_1 \rightarrow \tau_2$ as follows

$$\mathcal{H}X = \begin{cases} \mathcal{E}X, & \text{if } X \text{ is a tesseract} \\ \mathcal{L}X, & \text{if } X \text{ is a cubic pyramid or bipentatope.} \end{cases}$$

Then

$$\tau_{k+1} = \mathcal{H}^k \tau_1.$$

Thus, we have a conforming sequence of successive hybrid finite element triangulations $\{\tau_k\}$.

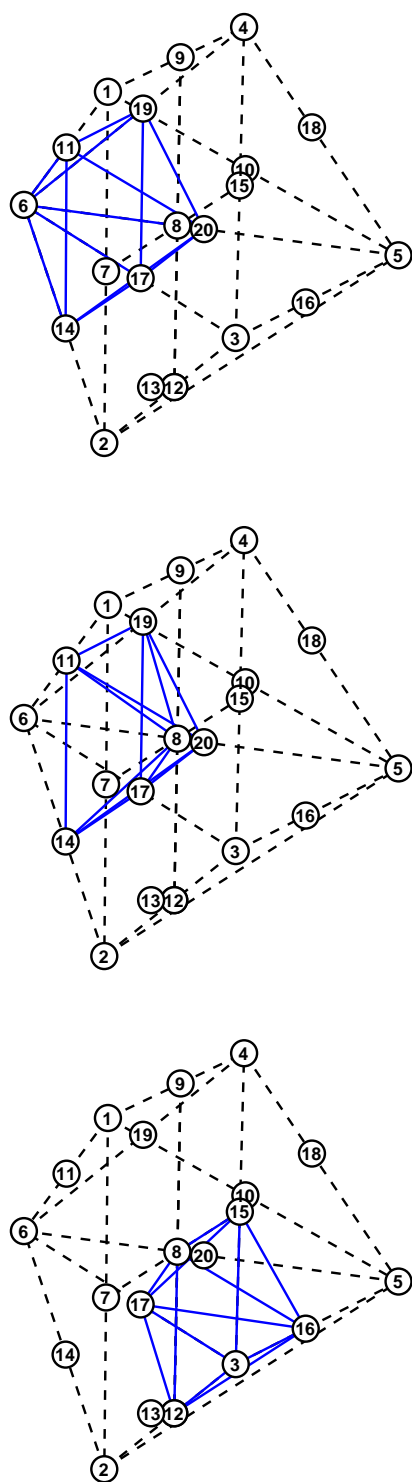


Fig. 11: The elements \mathbb{P}_2 , \mathbb{P}_4 , and \mathbb{P}_9 of the decomposition \mathcal{MP}^* .

4 Theoretical results

In this section, we summarize the important theoretical results that govern the hybrid triangulations introduced in the previous section.

Property 1 *The hypercube T^n can be divided into $2n$ hypercubic pyramids K_i^n so that all edges of the i -th pyramid have the same length.*

Theorem 1 *The four-dimensional space is the only Euclidean space that satisfies Property 1.*

Proof For the sake of simplicity, we suppose that

$$T^n = [t_1^n(-a, -a, \dots, -a), \dots, t_{2n}^n(a, a, \dots, a)]$$

has all edges parallel to the coordinate axes. Then, Property 1 is valid iff

$$\frac{1}{2}h[T^n] = l[T^n],$$

where $l[T^n]$ is the edge length of T^n . The latter equality leads to

$$\frac{1}{2}\sqrt{\sum_{k=1}^n (2a)^2} = 2a \Rightarrow \sqrt{na^2} = 2a,$$

which is possible iff $n = 4$. □

The result of Theorem 1 is that the four-dimensional space is unique among all Euclidean spaces.

Theorem 2 *Consider the cubic pyramids in \mathcal{DK}^* . All such pyramids are congruent to the reference pyramid, i.e. $\mathbb{K}_i \subset [K^*]$, $i = 1, 2, \dots, 10$.*

Proof For all elements \mathbb{K}_i $i = 1, 2, \dots, 10$, of \mathcal{DK}^* it is possible to verify through direct calculation that:

- (i) all edges of \mathbb{K}_i are equal to 1;
- (ii) the base of \mathbb{K}_i is a cube with edges equal to 1;
- (iii) the degeneracy measure of \mathbb{K}_i is $\delta(\mathbb{K}_i) = 4.18154$;

from which congruency with the reference pyramid follows. □

Theorem 3 *Consider the bipentatopes in \mathcal{DK}^* . All such bipentatopes are congruent.*

Proof Without loss of generality, we consider demonstrating this property for two bipentatopes chosen from \mathcal{DK}^* , with the claim following from repeating this procedure for all pairwise combinations. With this in mind, we take our two bipentatopes chosen from \mathcal{DK}^* to be P_{10} and P_{14} , see Figure 9. Any

bipentatope can be partitioned into two pentatopes as shown in Figure 4. We hence begin by dividing the bipentatopes P_{10} and P_{14} into pentatopes whence

$$\begin{aligned} P_{10} &= \hat{S}_{10} [p_{15}, p_{18}, p_{19}, p_{20}, p_{35}] \cup \check{S}_{10} [p_{14}, p_{15}, p_{18}, p_{20}, p_{35}], \\ P_{14} &= \hat{S}_{14} [p_{15}, p_{28}, p_{29}, p_{33}, p_{36}] \cup \check{S}_{14} [p_{15}, p_{28}, p_{29}, p_{35}, p_{36}]. \end{aligned}$$

Let the generic affine transformations of the pentatopes \hat{S}_{10} and \hat{S}_{14} be

$$F_{10} : \hat{S}_{10} = A_{10}\mathcal{S}^* + B_{10}, \quad F_{14} : \hat{S}_{14} = A_{14}\mathcal{S}^* + B_{14}.$$

We map \hat{S}_{14} onto \hat{S}_{10} by

$$\hat{S}_{10} = F_{10} \left(F_{14}^{-1} \left(\hat{S}_{14} \right) \right) \Leftrightarrow F_{14,10} : \hat{S}_{10} = A_{14,10}\hat{S}_{14} + B_{10} - A_{14,10}B_{14},$$

where $A_{14,10}$ is the transitional matrix from \hat{S}_{14} to \hat{S}_{10} and $F_{14,10} = F_{10} \circ F_{14}^{-1}$. We emphasize that $p_{14} = F_{14,10}(p_{35})$, which assures that $P_{10} = F_{14,10}(P_{14})$. The claim that $P_{10} \cong P_{14}$ follows from the fact that the transition matrix

$$A_{14,10} = \begin{pmatrix} -1 & 0 & 0 & 0 \\ 0 & 0 & 1 & 0 \\ 0 & -1 & 0 & 0 \\ 0 & 0 & 0 & -1 \end{pmatrix}$$

is orthogonal. \square

Remark 1 *Let all bipentatopes from \mathcal{DK}^* be partitioned into two pentatopes as it is shown in Figure 4. Then all of them belong to $[\hat{S}_{10}]$ and $\delta([\hat{S}_{10}]) = 5$. Moreover, the elements of $[\hat{S}_{10}]$ are invariant. For more details concerning this class of pentatopes, we refer the reader to [30].*

Theorem 4 *Consider the bipentatopes in \mathcal{MP}^* . All such bipentatopes are congruent to the reference bipentatope, i.e. $\mathbb{P}_j \subset [P^*]$, $j = 1, 2, \dots, 16$.*

Proof Firstly, we prove that all bipentatopes in \mathcal{MP}^* belong to the same class. We randomly choose two bipentatopes \mathbb{P}_2 and \mathbb{P}_4 (see Figure 11) from \mathcal{MP}^* . The bipentatope \mathbb{P}_2 is obtained by the coupling of the pentatopes

$$\hat{S}_2 [p_6, p_{11}, p_{14}, p_{17}, p_{20}] \quad \text{and} \quad \check{S}_2 [p_6, p_{11}, p_{17}, p_{19}, p_{20}].$$

The second bipentatope is partitioned as follows

$$\mathbb{P}_4 = \hat{S}_4 [p_8, p_{11}, p_{14}, p_{17}, p_{20}] \cup \check{S}_4 [p_8, p_{11}, p_{17}, p_{19}, p_{20}].$$

The pentatope \hat{S}_2 is mapped onto \hat{S}_4 by the affine transformation

$$\hat{S}_4 = F_4 \left(F_2^{-1} \left(\hat{S}_2 \right) \right),$$

where

$$F_2 : \hat{S}_2 = A_2\mathcal{S}^* + B_2, \quad F_4 : \hat{S}_4 = A_4\mathcal{S}^* + B_4.$$

We present the map $F_{2,4} = F_4 \circ F_2^{-1}$ in a matrix form by

$$F_{2,4} : \hat{S}_4 = A_{2,4}\hat{S}_2 + B_4 - A_{2,4}B_4.$$

The transitional matrix

$$A_{2,4} = \begin{pmatrix} 1 & 0 & 0 & 0 \\ 0 & 0 & 0 & -1 \\ 0 & 0 & 1 & 0 \\ 0 & -1 & 0 & 0 \end{pmatrix}$$

is orthogonal. Additionally, $F_{2,4}$ keeps the facet $\mathbb{P}_{2,-1,-6}$ invariant, which assures $\mathbb{P}_4 = F_{2,4}(\mathbb{P}_2)$. Therefore, $\mathbb{P}_2 \cong \mathbb{P}_4$.

On the other hand, all edges of the bipentatopes have the same length equal to $\frac{1}{2}$, i.e. they are identical.

It remains to prove that \mathbb{P}_2 belongs to $[P^*]$. This follows directly from $A_{2,*} = 2I$, where $A_{2,*}$ is the transitional matrix from \mathbb{P}_2 to P^* and I is the identity matrix. \square

5 Quadrature rules for the cubic pyramid

5.1 Methodology

In this section, we consider the problem of approximating the integral of a function $f(\mathbf{x})$ on K^* , the reference cubic pyramid. This can be effectively accomplished via a quadrature rule whence

$$\int_{-1}^0 \int_{x_4}^{-x_4} \int_{x_4}^{-x_4} \int_{x_4}^{-x_4} f(\mathbf{x}) dx_1 dx_2 dx_3 dx_4 \approx \sum_{j=1}^N \omega_j f(\mathbf{x}_j), \quad (4)$$

where $\{\omega_j\}$ are a set of N weights and $\{\mathbf{x}_j\}$ are an associated set of N points—known as abscissa—which together specify a *quadrature rule*. If a rule is capable of exactly computing the integrals of a generic constant and all polynomials in the set

$$\Xi(p) = \{\psi_{ijkq}(\mathbf{x}) \mid 0 < i + j + k + q \leq p \text{ and } i, j, k, q \geq 0\},$$

where $\psi_{ijkq}(\mathbf{x})$ is as given in Eq. (1), then the rule is said to be of strength p . When defining the abscissa of a rule, it is typical to constrain them to be strictly inside of our domain and be arranged symmetrically. This ensures that we never evaluate $f(\mathbf{x})$ outside of its domain. In addition, to reduce the likelihood of catastrophic cancellation it is also customary to require the weights to be positive. Evidently if the rule is to integrate a generic constant mode correctly it must necessarily be the case that

$$\sum_{j=1}^N \omega_j = 2.$$

Substituting the polynomials from our set into Eq. (4) and enforcing equality we require for all $\psi \in \Xi(p)$ that

$$\int_{-1}^0 \int_{x_4}^{-x_4} \int_{x_4}^{-x_4} \int_{x_4}^{-x_4} \psi(\mathbf{x}) dx_1 dx_2 dx_3 dx_4 = 0 = \sum_{j=1}^N \omega_j \psi(\mathbf{x}_j),$$

where in evaluating the integral we have exploited the orthogonality relationship associated with the polynomials in our basis. This can be regarded as a non-linear least squares problem in which we have $|\Xi(p)| + 1$ equations and $5N$ unknowns. However, unlike a typical least squares problem, it is one where we seek a solution with zero residual. Assuming the abscissa are known we remark that the associated weights may be determined through the solution of a *linear* least squares problem. This enables us to reduce the number of degrees of freedom in our non-linear problem to $4N$.

In order to enforce symmetry, it is advantageous to decompose our N abscissa into symmetry orbits. The symmetry orbits of the cubic pyramid are similar to those of the hexahedron, with an additional parameter that accounts for the extent of the pyramid in the fourth dimension. Therefore, one may follow the procedure for generating orbits for the hexahedron (see [40]), and enumerate all symmetry orbits. Thereafter, upon adding a parameter to account for the fourth dimension, the symmetry orbits of the cubic pyramid are written as follows

$$\begin{aligned} S_1(\delta) &= (0, 0, 0, \delta), & |S_1| &= 1, \\ S_2(\alpha, \delta) &= \chi(\alpha, 0, 0, \delta), & |S_2| &= 6, \\ S_3(\alpha, \delta) &= \chi(\alpha, \alpha, \alpha, \delta), & |S_3| &= 8, \\ S_4(\alpha, \delta) &= \chi(\alpha, \alpha, 0, \delta), & |S_4| &= 12, \\ S_5(\alpha, \beta, \delta) &= \chi(\alpha, \beta, 0, \delta), & |S_5| &= 24, \\ S_6(\alpha, \beta, \delta) &= \chi(\alpha, \alpha, \beta, \delta), & |S_6| &= 24, \\ S_7(\alpha, \beta, \gamma, \delta) &= \chi(\alpha, \beta, \gamma, \delta), & |S_7| &= 48, \end{aligned}$$

subject to the constraints $0 < \alpha, \beta, \gamma \leq -\delta$ and $-1 \leq \delta \leq 0$. Here, the operator χ returns all possible (unique) signed permutations of the input arguments.

Now, let us provide an example of how these symmetry orbits are used. If $N = 156$, then one possible arrangement of points is four S_1 orbits, two S_2 orbits, one S_3 orbit, three S_4 orbits, two S_5 orbits, and one S_7 orbit whence

$$N = 4|S_1| + 2|S_2| + |S_3| + 3|S_4| + 2|S_5| + |S_7| = 156,$$

as required. Inspecting the number of arguments for each of the orbits and summing we find that this decomposition has a total of 26 degrees of freedom. Together these fix the locations of all of our abscissa and hence become the parameters in our non-linear least squares problem. We note here that this represents a substantial decrease compared with an asymmetric rule which has some $4N = 624$ degrees of freedom. Of course, for a given N there are

typically a very large number of distinct decompositions into symmetry orbits. For our example of $N = 156$ there are some 8518 unique decompositions.

Our overall goal when identifying quadrature rules is to find one with the minimum value of N for a particular strength p . Unfortunately, given a p it is not possible to determine N theoretically; instead it must be treated as a hyper-parameter to the overall optimisation process. Similarly, once given an N it is, in general, not possible to know *a priori* which particular symmetric decomposition will yield a rule—if any. Thus, it is also necessary to treat the specific decomposition as a hyper-parameter, too.

We have implemented the aforementioned system into the open source symmetric quadrature rule package Polyquad [40]. Running this modified version of Polyquad on a workstation, we have identified symmetric quadrature rules on the cubic pyramid for $2 \leq p \leq 12$. The total number of points required for these rules can be seen in Table 1. The abscissa for all of our rules are inside of our reference pyramid, and feature positive weights. The rules themselves are provided in quadruple precision in the electronic supplemental material. An example of the $p = 5$ quadrature rule is provided in Table 2.

Table 1: Number of points N required for a rule of strength p inside of the cubic pyramid.

p	2	3	4	5	6	7	8	9	10	11	12
N	7	10	21	29	50	65	114	163	251	323	552

Table 2: The $p = 5$ quadrature rule on the cubic pyramid K^* with $N = 29$ points. The remaining rules are provided in the electronic supplemental material.

Orbit	Abscissa	Weight
S_1	-0.32846339581882957902277574789024	0.084184481885656624083314191434215
S_2	0.59942266549153142521578075246447 -0.74912930534502345701037962143888	0.11340384654119720346152792514806
S_2	0.76070275297226284532398968584027 -0.95754362470717092670167055158225	0.089004419809134534555110633350815
S_3	0.43384835705078179649267535015814 -0.5766200661792940506119682920933	0.033983660519520996993103370708523
S_3	0.69719510426558290268820473081072 -0.91852788682445245487884982935091	0.05368707948202312148400343648805

5.2 Numerical experiments

The objective of this section is to numerically validate a subset of the quadrature rules in Table 1. Towards this end, we performed a series of numerical

experiments on the rules with strengths $p = 2, 3, \dots, 9$. These rules are capable of exactly integrating certain monomial functions by construction, as well as approximately integrating certain transcendental functions. In what follows, we limit our focus to: a) weighted combinations of monomial functions, and b) analytic transcendental functions. In addition, we execute all of the numerical experiments in quadruple precision arithmetic in order to demonstrate the full precision of the rules.

5.2.1 Polynomial integration

In this section, we evaluate the ability of our quadrature rules to integrate a weighted combination of monomial functions on the reference cubic pyramid K^* . More specifically, we consider the following polynomial function of degree m

$$f_{\text{poly}}(\mathbf{x}; m) = \sum_{r=0}^m \sum_{s=0}^{m-r} \sum_{t=0}^{m-r-s} \sum_{v=0}^{m-r-s-t} C_{rstv} x_1^r x_2^s x_3^t x_4^v,$$

where the constants C_{rstv} are given by the following formula

$$C_{rstv} = 24 \frac{(r+1)(s+1)(t+1)(v+1)}{(m+1)(m+2)(m+3)(m+4)}.$$

One may observe that this function contains all possible distinct monomials of degree m . It turns out that the integral of this function on the domain K^* can be computed exactly as follows

$$J_{\infty}(\mathbf{x}; m) = \int_{K^*} f_{\text{poly}}(\mathbf{x}) d\mathbf{x} = \sum_{r=0}^m \sum_{s=0}^{m-r} \sum_{t=0}^{m-r-s} \sum_{v=0}^{m-r-s-t} C_{rstv} I_{rstv},$$

where

$$I_{rstv} = \int_{K^*} x_1^r x_2^s x_3^t x_4^v d\mathbf{x} = \frac{(1+(-1)^r)(1+(-1)^s)(1+(-1)^t)(-1)^v}{(1+r)(1+s)(1+t)(r+s+t+v+4)},$$

is the exact integral of each monomial.

The approximate integral of f_{poly} can be computed by evaluating the following quadrature formula

$$J_p = \sum_{j=1}^N \omega_j f_{\text{poly}}(\mathbf{x}_j),$$

where the number of points $N = N(p)$, weights $\omega_j = \omega_j(p)$, and abscissa $\mathbf{x}_j = \mathbf{x}_j(p)$ are functions of the quadrature rule strength p . Evidently, we obtain exact integration $J_p = J_{\infty}$ when $p \geq m$, and approximate integration $J_p \approx J_{\infty}$ when $p < m$.

Figure 12 shows the quadrature error produced by integrating f_{poly} for different values of m and p . In accordance with expectations, we obtain exact integration whenever $p \geq m$, to within machine precision (10^{-32}).

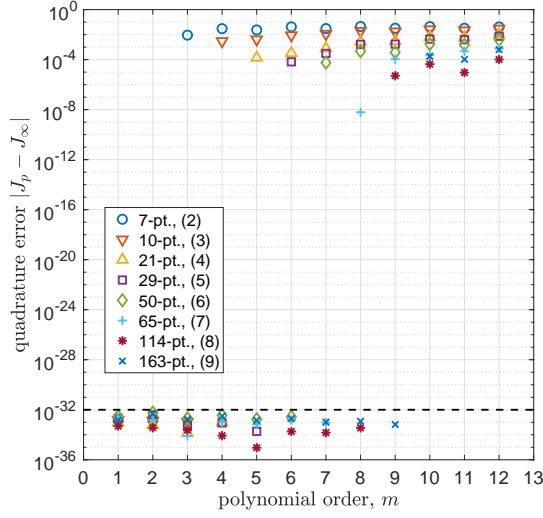


Fig. 12: Absolute error in the numerical integration of f_{poly} over the reference cubic pyramid K^* . The dashed line marks the threshold of machine precision.

5.2.2 Transcendental integration

In this section, we evaluate the ability of our quadrature rules to integrate a set of transcendental functions on a family of successively refined meshes. For this purpose, we consider the following functions

$$f_1(\mathbf{x}) = \sin(\pi x_1^2) \sin(\pi x_2^2) \sin(\pi x_3^2) \sin(\pi x_4^2),$$

$$f_2(\mathbf{x}) = \exp(x_1^2) \exp(x_2^2) \exp(x_3^2) \exp(x_4^2),$$

$$f_3(\mathbf{x}) = \exp(x_1) \exp\left(\frac{1}{2}x_2\right) \exp\left(\frac{1}{3}x_3\right) \exp\left(\frac{1}{4}x_4\right).$$

Note that the first two functions are symmetric with respect to the coordinates x_1, \dots, x_4 , whereas the last function is asymmetric.

The integral of each transcendental function was computed on the domain $\Omega = [0, 1]^4$ as follows

$$J_\infty = \int_{\Omega} f_{\text{trans}}(\mathbf{x}) d\mathbf{x}.$$

The analytical solution of this integral is generally unknown. As a result, the ‘exact’ integration was carried out using a vectorized adaptive integration routine in Matlab. This routine approximates the integral of a smooth function to an arbitrary level of precision by successively subdividing the domain of integration, and leveraging nested Gauss-Kronrod quadrature rules to estimate the integration error on each subinterval. One may consult the work of

Shampine [33,34] for details of the Matlab implementation, and Notaris [27] for a general review of Gauss-Kronrod quadrature rules. In our case, we used the adaptive Matlab routine to approximate the integrals to within machine precision.

The transcendental functions above were also integrated using the aforementioned quadrature rules on the cubic pyramid. In order to facilitate this process, the domain Ω was covered with a uniform mesh of M^4 tesseract elements where M is a positive integer. Thereafter, each tesseract was subdivided into 8 cubic pyramid elements in accordance with the partition operator \mathcal{B} , yielding a total of $N_e = 8M^4$ cubic pyramid elements. The quadrature rules were transformed (mapped) from the reference cubic pyramid K^* to the individual cubic pyramids in the mesh via a linear mapping procedure. The approximate integral of each function was then computed in the following fashion

$$J_p = \sum_{i=1}^{N_e} \sum_{j=1}^N \omega_j^{K_i} f_{\text{trans}}(\mathbf{x}_j^{K_i}),$$

where $\omega_j^{K_i}$ are the quadrature weights and $\mathbf{x}_j^{K_i}$ are the point locations in each element K_i .

Figures 13, 14, and 15 illustrate the quadrature errors for integrating f_1 , f_2 , and f_3 on Ω for mesh parameters $M = 1, 2, \dots, 10$. In each case, the error converges at a rate of h^{p+1} or higher. In addition, the pairs of even and odd quadrature rules converge at the same rates, e.g. rules with $p = 2$ and $p = 3$ converge at a rate of h^4 . Upon combining these insights together, we estimate that the rules will typically converge at a rate of h^{p+2} for even values of p , and h^{p+1} for odd values of p . The precise reason for this behavior is unknown, although it is likely due to fortunate cancellations of truncation error terms for quadrature rules with even values of p .

In addition, we note that increasing the number of quadrature points (by increasing p) does not always yield a more accurate result when integrating transcendental functions. For example, the 50 point rule with $p = 6$ sometimes outperforms the 65 point rule with $p = 7$ (see Figure 15). This behavior is likely due to a convenient alignment between the symmetry orbits of the $p = 6$ rule and the local topology of the transcendental function f_3 . We note that this trend is not general, as it does not hold for f_1 and f_2 . In fact, in most cases the higher degree rules outperform the lower degree rules, as expected.

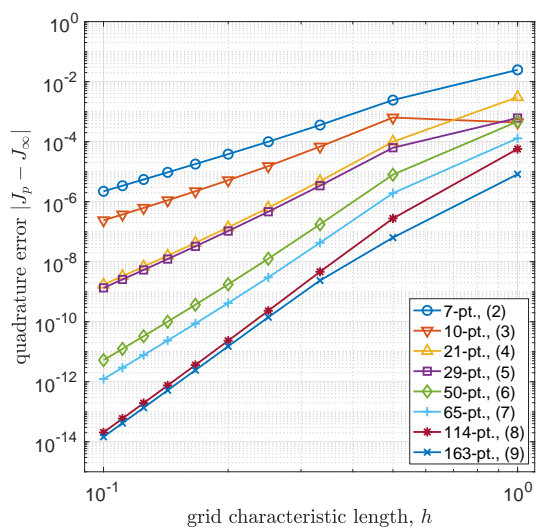


Fig. 13: Absolute value of the error in the numerical integration of f_1 over the domain Ω for mesh parameters $M = 1, 2, \dots, 10$.

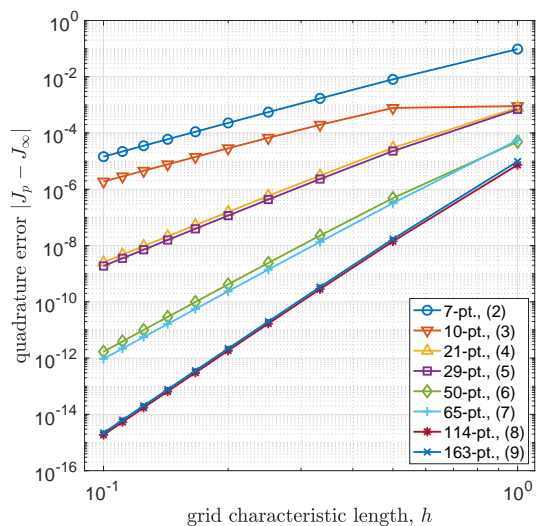


Fig. 14: Absolute value of the error in the numerical integration of f_2 over the domain Ω for mesh parameters $M = 1, 2, \dots, 10$.

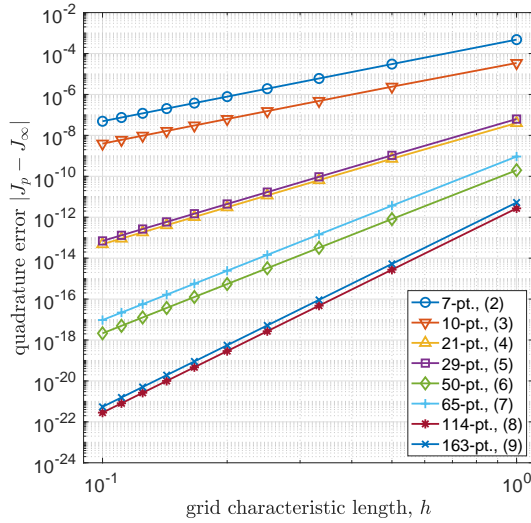


Fig. 15: Absolute value of the error in the numerical integration of f_3 over the domain Ω for mesh parameters $M = 1, 2, \dots, 10$.

6 Conclusion

In this work, we have presented a novel refinement strategy for four-dimensional cubic pyramids. Given a cubic pyramid our method subdivides it into a conforming set of smaller cubic pyramids and bipentatopes. Moreover, all of the edges of each cubic pyramid have the same length, as do the edges of each bipentatope, which corresponds to an optimal configuration. Furthermore, we have also developed and evaluated a new set of polynomial quadrature rules inside of the cubic pyramid. Together, these results open up new pathways for four-dimensional meshing for space-time finite element methods.

For the sake of completeness, we also provided a comprehensive example of a four-dimensional conformal hybrid mesh on a canonical domain. The initial mesh contains tesseract and cubic pyramid elements. The mesh is conformal because the couplings between the tesseracts and the cubic pyramids are consistent, without the need for an interface subdomain. Following the formation of the initial mesh, it is refined by subdividing the tesseract elements in the standard fashion (splitting along planes that are orthogonal to the coordinate axes), and by subdividing the cubic pyramids in the aforementioned novel fashion. We believe that this strategy can be generalized to a much broader class of hybrid meshes, including curved meshes, without significant modifications.

Declarations

Funding

The authors did not receive support from any organization for the submitted work.

Conflict of interest/Competing interests

The authors have no conflicts of interest to declare that are relevant to the content of this article.

Availability of data and material

The quadrature rules are available as electronic supplemental material.

Code availability

The Polyquad code is available at <https://github.com/PyFR/Polyquad>.

References

1. Ainsworth, M., Fu, G.: A lowest-order composite finite element exact sequence on pyramids. *Computer Methods in Applied Mechanics and Engineering* **324**, 110–127 (2017)
2. Arnold, D., Falk, R., Winther, R.: Finite element exterior calculus: from Hodge theory to numerical stability. *Bulletin of the American Mathematical Society* **47**(2), 281–354 (2010)
3. Arnold, D.N., Falk, R.S., Winther, R.: Finite element exterior calculus, homological techniques, and applications. *Acta Numerica* **15**, 1 (2006)
4. Bedrosian, G.: Shape functions and integration formulas for three-dimensional finite element analysis. *International Journal for Numerical Methods in Engineering* **35**(1), 95–108 (1992)
5. Bergot, M., Cohen, G., Duruflé, M.: Higher-order finite elements for hybrid meshes using new nodal pyramidal elements. *Journal of Scientific Computing* **42**(3), 345–381 (2010)
6. Brandts, J., Korotov, S., Krížek, M.: Simplicial finite elements in higher dimensions. *Applications of Mathematics* **52**(3), 251–265 (2007)
7. Cao, C., Qin, Q.H., Yu, A.: A new hybrid finite element approach for three-dimensional elastic problems. *Archives of Mechanics* **64**(3), 261–292 (2012)
8. Caplan, P.C.: Four-dimensional anisotropic mesh adaptation for spacetime numerical simulations. Ph.D. thesis, Massachusetts Institute of Technology (2019)
9. Chan, J., Warburton, T.: A comparison of high order interpolation nodes for the pyramid. *SIAM Journal on Scientific Computing* **37**(5), A2151–A2170 (2015)
10. Chan, J., Warburton, T.: hp-finite element trace inequalities for the pyramid. *Computers & Mathematics with Applications* **69**(6), 510–517 (2015)
11. Chan, J., Warburton, T.: Orthogonal bases for vertex-mapped pyramids. *SIAM Journal on Scientific Computing* **38**(2), A1146–A1170 (2016)
12. Chan, J., Warburton, T.: A short note on a Bernstein–Bezier basis for the pyramid. *SIAM Journal on Scientific Computing* **38**(4), A2162–A2172 (2016)
13. Coulomb, J.L., Zgainski, F.X., Marechal, Y.: A pyramidal element to link hexahedral, prismatic and tetrahedral edge finite elements. *IEEE Transactions on Magnetics* **33**(2), 1362–1365 (1997)

14. Coxeter, H.: Regular and semi-regular polytopes. I. *Mathematische Zeitschrift* **46**(1), 380–407 (1940)
15. Coxeter, H.S.M.: *Regular Polytopes*. Courier Corporation (1973)
16. Devloo, P.R., Duran, O., Gomes, S.M., Ainsworth, M.: High-order composite finite element exact sequences based on tetrahedral–hexahedral–prismatic–pyramidal partitions. *Computer Methods in Applied Mechanics and Engineering* **355**, 952–975 (2019)
17. Dumont, S., Jourdan, F.: A space-time finite element method for elastodynamics problems with a moving loading zone. In: *Eleventh International Conference on Computational Structures Technology* (2012)
18. Frontin, C.V., Walters, G.S., Witherden, F.D., Lee, C.W., Williams, D.M., Darmofal, D.L.: Foundations of space-time finite element methods: polytopes, interpolation, and integration. *arXiv preprint arXiv:2012.08701* (2020)
19. Gillette, A.: Serendipity and tensor product affine pyramid finite elements. *The SMAI Journal of Computational Mathematics* **2**, 215–228 (2016)
20. Korotov, S., Křížek, M.: Red refinements of simplices into congruent subsimplices. *Computers & Mathematics with Applications* **67**(12), 2199–2204 (2014)
21. Langer, U., Steinbach, O.: *Space-Time Methods: Applications to Partial Differential Equations*, vol. 25. Walter de Gruyter GmbH & Company (2019)
22. Maday, Y., Mavriplis, C., Patera, A.: Nonconforming mortar element methods: Application to spectral discretizations. In: *Domain decomposition methods: Proceedings of the Second International Symposium*, pp. 392–418 (1988)
23. McLaren-Young-Sommerville, D.: *An Introduction to the Geometry of n Dimensions*. Dover (1958)
24. Meshkat, S., Talmor, D.: Generating a mixed mesh of hexahedra, pentahedra and tetrahedra from an underlying tetrahedral mesh. *International Journal for Numerical Methods in Engineering* **49**(1-2), 17–30 (2000)
25. Neumüller, M., Karabelas, E.: Generating admissible space-time meshes for moving domains in (d+1) dimensions. In: *Space-Time Methods: Applications to Partial Differential Equations*, pp. 185–206 (2019)
26. Nigam, N., Phillips, J.: Numerical integration for high order pyramidal finite elements. *ESAIM: Mathematical Modelling and Numerical Analysis-Modélisation Mathématique et Analyse Numérique* **46**(2), 239–263 (2012)
27. Notaris, S.E.: Gauss-Kronrod quadrature formulae—A survey of fifty years of research. *Electronic Transactions on Numerical Analysis* **45**, 371–404 (2016)
28. Pantano, A., Averill, R.C.: A penalty-based interface technology for coupling independently modeled 3D finite element meshes. *Finite Elements in Analysis and Design* **43**(4), 271–286 (2007)
29. Petrov, M.S., Todorov, T.D.: Stable subdivision of 4D polytopes. *Numerical Algorithms* **79**(2), 633–656 (2018)
30. Petrov, M.S., Todorov, T.D.: Properties of the multidimensional finite elements. *Applied Mathematics and Computation* (2020). In Press
31. Reberol, M., Lévy, B.: Low-order continuous finite element spaces on hybrid non-conforming hexahedral-tetrahedral meshes. *arXiv preprint arXiv:1605.02626* (2016)
32. Seshaiyer, P., Suri, M.: hp submeshing via non-conforming finite element methods. *Computer Methods in Applied Mechanics and Engineering* **189**(3), 1011–1030 (2000)
33. Shampine, L.F.: Matlab program for quadrature in 2D. *Applied Mathematics and Computation* **202**(1), 266–274 (2008)
34. Shampine, L.F.: Vectorized adaptive quadrature in Matlab. *Journal of Computational and Applied Mathematics* **211**(2), 131–140 (2008)
35. Steinbach, O.: Space-time finite element methods for parabolic problems. *Computational Methods in Applied Mathematics* **15**(4), 551–566 (2015)
36. Steinbach, O., Yang, H.: An algebraic multigrid method for an adaptive space–time finite element discretization. In: *International Conference on Large-Scale Scientific Computing*, pp. 66–73. Springer (2017)
37. Todorov, T.D.: The optimal refinement strategy for 3-D simplicial meshes. *Computers & Mathematics with Applications* **66**(7), 1272–1283 (2013)
38. Touloupoulos, I.: Space-time finite element methods stabilized using bubble function spaces. *Applicable Analysis* **99**(7), 1153–1170 (2020)

39. Williams, D.M., Frontin, C.V., Miller, E.A., Darmofal, D.L.: A family of symmetric, optimized quadrature rules for pentatopes. *Computers & Mathematics with Applications* **80**(5), 1405–1420 (2020)
40. Witherden, F.D., Vincent, P.E.: On the identification of symmetric quadrature rules for finite element methods. *Computers & Mathematics with Applications* **69**(10), 1232–1241 (2015)
41. Yamakawa, S., Gentilini, I., Shimada, K.: Subdivision templates for converting a non-conformal hex-dominant mesh to a conformal hex-dominant mesh without pyramid elements. *Engineering with Computers* **27**(1), 51–65 (2011)
42. Yamakawa, S., Shimada, K.: Increasing the number and volume of hexahedral and prism elements in a hex-dominant mesh by topological transformations. In: *Proceedings of the 12th International Meshing Roundtable*, pp. 403–413 (2003)
43. Yamakawa, S., Shimada, K.: Converting a tetrahedral mesh to a prism–tetrahedral hybrid mesh for FEM accuracy and efficiency. *International Journal for Numerical Methods in Engineering* **80**(1), 74–102 (2009)
44. Yamakawa, S., Shimada, K.: 88-Element solution to Schneiders’ pyramid hex-meshing problem. *International Journal for Numerical Methods in Biomedical Engineering* **26**(12), 1700–1712 (2010)
45. Yamakawa, S., Shimada, K.: Automatic all-hex mesh generation of thin-walled solids via a conformal pyramid-less hex, prism, and tet mixed mesh. In: *Proceedings of the 20th International Meshing Roundtable*, pp. 125–141. Springer (2011)
46. Zamboj, M.: Sections and shadows of four-dimensional objects. *Nexus Network Journal* **20**(2), 475–487 (2018)